Unified description of potential profiles and electrical transport in unipolar and ambipolar organic field-effect transistors

Smits, Edsger C. P.; Mathijssen, Simon G. J.; Colle, Michael; Mank, Arjan J. G.; Bobbert, Peter A.; Blom, Paul W. M.; de Boer, Bert; de Leeuw, Dago M.; Cölle, Michael

Published in:
Physical Review. B: Condensed Matter and Materials Physics

DOI:
10.1103/PhysRevB.76.125202

Publication date:
2007

Unified description of potential profiles and electrical transport in unipolar and ambipolar organic field-effect transistors

Edsger C. P. Smits,[1,2,3,*] Simon G. J. Mathijssen,[2,4] Michael Cölle,[2] Arjan J. G. Mank,[2] Peter A. Bobbert,[4] Paul W. M. Blom,[1] Bert de Boer,[1] and Dago M. de Leeuw[2]

[1]*Molecular Electronics, Zernike Institute of Advanced Materials, University of Groningen, Nijenborgh 4, 9747 AG Groningen, The Netherlands*

[2]*Philips Research Laboratories, High Tech Campus 4 (WAG 11), 5656 AE Eindhoven, The Netherlands*

[3]*Dutch Polymer Institute (DPI), P.O. Box 902, 5600 AX Eindhoven, The Netherlands*

[4]*Department of Applied Physics, Eindhoven University of Technology, P.O. Box 513, 5600 MB Eindhoven, The Netherlands*

(Received 17 April 2007; revised manuscript received 7 June 2007; published 7 September 2007)

Validation of models for charge transport in organic transistors is fundamentally important for their technological use. Usually current-voltage measurements are performed to investigate organic transistors. *In situ* scanning Kelvin probe microscopy measurements provide a powerful complementary technique to distinguish between models based on band and hopping transports. We perform combined current-voltage and Kelvin probe microscopy measurements on unipolar and ambipolar organic field-effect transistors. We demonstrate that by this combination we can stringently test these two different transport models and come up with a unified description of charge transport in disordered organic semiconductors.

DOI: 10.1103/PhysRevB.76.125202 PACS number(s): 73.50.Gr, 73.61.Ph

I. INTRODUCTION

Organic field-effect transistors (OFETs) have made tremendous progress in performance and reliability. Integrated circuits combining several thousands of transistors were realized.[1] The first active matrix displays[2] and contactless rf identification transponders have been demonstrated.[3,4] These devices are predominantly based on unipolar transistors. Design of integrated circuits requires models describing unipolar charge transport that can be introduced in circuit simulators.[5] Analytical models for the dc current-voltage characteristics in accumulation have been reported.[6] For disordered organic semiconductors, they are typically based on a mobility that increases with charge-carrier density, as derived from transport models based on variable-range hopping, i.e., thermally activated tunneling between localized states.[7] Classical metal-oxide-semiconductor (MOS) models with a constant mobility have also been presented.[8–10] However, in that case, empirical fit constants of unknown origin are required to describe charge transport.[11–14]

Charge transport models are also required for ambipolar transistors, particularly in the case of ambipolar light emitting transistors.[15–18] Here, electrons and holes are injected from opposite sides of the channel using a single type of source and drain electrodes. When the recombination rate is infinite, the device is described as a discrete *p*-type and *n*-type transistor in series. For verification of the underlying physics in both unipolar and ambipolar transistors, a complementary measuring method is needed.[19]

Noncontact or Kelvin probe potentiometry measures surface potentials.[20] For transistors based on unintentionally doped semiconductors, this potential is a measure of the potential at the semiconductor/gate-dielectric interface. This is schematically depicted in Fig. 1. Scanning Kelvin probe microscopy (SKPM) can, therefore, be used to determine the potential profile within the accumulation channel.[21–23] For unipolar transistors, SKPM has shown to be a powerful method to characterize grain boundaries and contact resistances.[20,24,25] The potential profile is directly related to the current-voltage characteristics. Therefore, SKPM is ideally suited to determine the internal consistency of charge transport models. Theoretical predictions of potential profiles, however, are scarce. In this paper, we derive simultaneously the current-voltage characteristics and the potential profiles for both unipolar and ambipolar OFETs.

II. EXPERIMENT

OFETs were fabricated using heavily doped *p*-type Si wafers as common gate electrode with a 200 nm thermally oxidized SiO_2 layer as gate dielectric. Using conventional photolithographic methods, gold source and drain electrodes were defined in a bottom contact, circular transistor configuration with channel width (W) and length (L) of 2500 and 10 μm, respectively. A 10 nm layer of titanium was used as adhesion layer for the gold on SiO_2. The SiO_2 layer was treated with the primer hexamethyldisilazane prior to semiconductor deposition in order to passivate its surface.[26] For unipolar transistors, films of poly(triarylamine) (PTAA) (Ref. 27) were spin coated from a toluene solution. As model com-

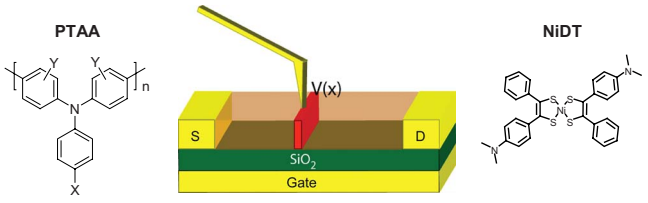

FIG. 1. (Color online) Schematic cross section of a field-effect transistor with gold source (S) and drain (D) electrodes. The SKPM tip probes the potential $V(x)$ at a specific position x parallel to the channel. Unipolar *p*-type transistors were made from PTAA and ambipolar transistors from the small band-gap molecule NiDT.

pound to analyze charge transport in ambipolar field-effect transistor, the small band-gap molecule nickel dithiolene (NiDT) was used.[28] The chemical formulas are presented in Fig. 1. For NiDT in contact with Au electrodes, the injection barriers for both electrons and holes are less than 0.5 eV and can be disregarded.[19] Film thicknesses were about 100 nm.

Scanning Kelvin probe microscopy measurements were performed *in situ* with a Veeco Dimension 3100 atomic force microscope (AFM) operated at ambient temperature in a dry nitrogen environment. First, the height profile was recorded in tapping mode. Then the potential profiles were measured in noncontact lift mode at a distance of 20 nm from the surface. The internal voltage sources of the AFM, coupled to a voltage amplifier (HP 6826A), were used to apply the biases to the electrodes. The surface potential was probed with a spatial resolution of about 100 nm.[25] The absolute values for the measured potentials depend on the type of tip used and the device geometry due to capacitive coupling. This leads to a small offset at the reference source and drain contacts. The effect is known in literature, and the potentials were corrected by scaling accordingly.[21] The accumulation layer in OFETs is located directly at the gate-dielectric/semiconductor interface.[29] Although the potentials are probed at a distance of 120 nm, viz., the film thickness plus the lift height, the potentials measured with SKPM are representative of the potentials in the channel, as confirmed by measuring at increased heights. Since the channel length is much larger than the semiconductor layer thickness, the associated stray fields can be disregarded. An ampere meter (Keithley 6485) was used to measure simultaneously the source-drain current. The sensitivity for the current measurements was a few picoamperes.

III. UNIPOLAR POTENTIAL PROFILES

The tip of the SKPM probes the local potential $V(x)$ at a certain position x in the channel parallel to the source-drain contacts. The difference between the local potential $V(x)$ and the gate bias V_g yields the effective gate potential $V_{eff}=V(x)-V_g+V_t$, where V_t is the threshold voltage. The amount of locally induced charge is given by the product of insulator capacitance C_i and effective gate bias. We assume that the charge-carrier mobility depends on the induced aerial charge density and, therefore, on the effective gate potential. More specifically, we take $\mu_{FET}(V_{eff})=f_0 V_{eff}^{\beta-2}$, where f_0 is a prefactor. The classical constant MOS mobility is obtained when β equals 2. For variable-range hopping, $\beta=2T_0/T$, where T_0 is a measure of the width of the exponential density of states and T is the absolute temperature.[7]

For the derivation of the current-voltage (I-V) characteristics, we consider long channels, so that short-channel effects and source and drain contact resistances can be disregarded. The gradual channel approximation can be used because the electric field perpendicular to the film is much larger than in the parallel (x) direction. First, we calculate the sheet conductance for each position x as a function of effective gate potential. The source-drain current in accumulation for a hole channel then follows from integration of the sheet conductances over the channel potential:[11–13,19]

$$I_{ds} = -\frac{WC_i}{L(\beta-1)}\int_0^{V_d} \mu_{FET} V_{eff} dV(x)$$

$$= -\frac{WC_i}{L}\frac{f_0}{\beta(\beta-1)}[(-V_g+V_t)^\beta - (V_d-V_g+V_t)^\beta]. \quad (1)$$

The potential profile $V(x)$ follows from current conservation. The current at each point x, $I_{ds}(x)$, is obtained by replacing in Eq. (1) V_d with $V(x)$ and L with x. Current conservation implies $I_{ds}=I_{ds}(x)$, from which $V(x)$ can be solved:

$$V(x) = V_g - V_t + \left\{(-V_g+V_t)^\beta - \frac{x}{L}[(-V_g+V_t)^\beta - (V_d-V_g+V_t)^\beta]\right\}^{1/\beta}. \quad (2)$$

Analysis of electrical transport, thus, yields values for β and V_t that are directly linked to the potential profile. The prefactor f_0 in Eq. (1) can be regarded as a scaling factor.

As a typical example, we characterized unipolar p-type PTAA transistors by current-voltage and *in situ* SKPM measurements. In Fig. 2(a), the symbols show the potentials measured in the channel as a function of applied gate bias. Figure 2(b) shows the corresponding measured transfer curve. The mobility is calculated to increase from 5×10^{-5} cm^2/V s at a gate bias of 0 V to 3×10^{-4} cm^2/V s at −18 V. The solid line in the inset is a fit to the experimental transfer curve using Eq. (1). A good fit was obtained for $V_t=7$ V, $\beta=2.7$, and $f_0=3.5\times10^{-5}$ cm^2/V$^{(2T_0/T-1)}$ s. The values of the fit constants are comparable to those reported in literature for other organic semiconductors.[26,29] With the same values for V_t and β, we calculated the potential profiles in Fig. 2(a) with Eq. (2). The fits are presented as solid lines. Without any additional parameter, excellent fits are obtained for all applied gate biases. Similarly, we measured the potential profiles and output currents at a gate bias of −7 V by sweeping the drain bias [Fig. 3(a)]. The symbols show the experimental data points. The solid lines are calculated using the same values for V_t and β as used in Figs. 2(a) and 2(b). Again, an excellent fit is obtained. Hence, both the output and transfer curves and the corresponding potential profiles can simultaneously be fitted. We also tried to fit the data using $\beta=2$, yielding the classical MOS equations.[10] As a typical example, we present the best fit for the potentials with a drain bias of −7 V and a gate bias of −9 V in Fig. 3(a) by the dashed line. No satisfying agreement could be obtained.

Qualitatively, the potential profiles can be explained as follows. In the linear regime when $|V_d| \ll |V_g|$, the charge density is only determined by the applied gate bias. The charge distribution, and hence the sheet conductance, is uniform over the channel. Therefore, the lateral field due to the small drain bias is constant and the potential profile is a straight line. When the drain bias cannot be neglected, the charge-carrier density distribution is not uniform. The carrier density depends on the effective gate potential and decreases from source to drain. The sheet conductance increases with carrier density. Hence the sheet conductance decreases from source to drain, and the lateral electric field increases mono-

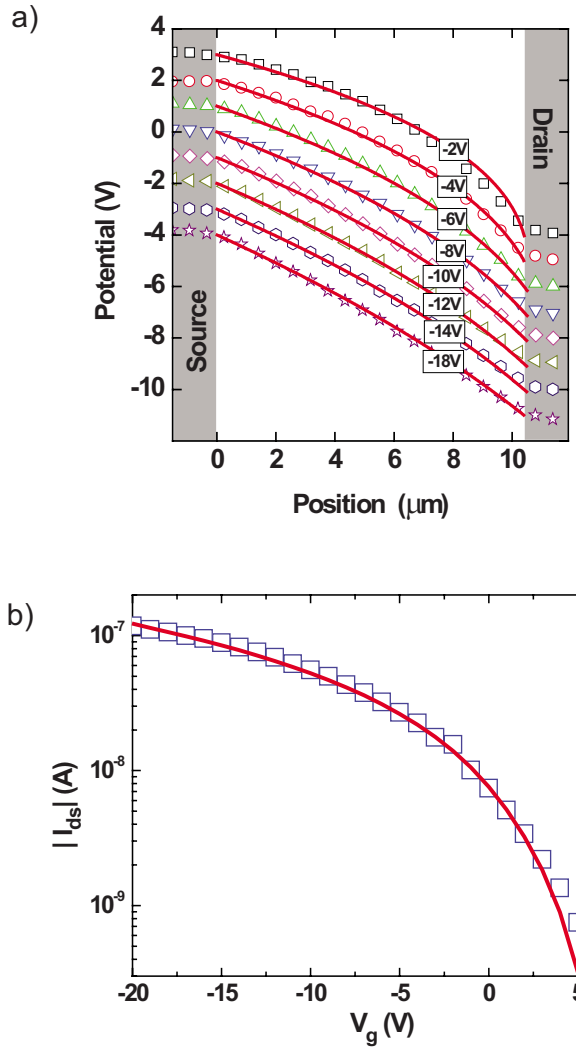

FIG. 2. (Color online) Transfer curves, together with the corresponding potential profiles, as measured for a unipolar PTAA field-effect transistor. Symbols and solid lines represent measured data points and fits, respectively. (a) The potential profiles measured at gate biases from −2 to −18 V in steps of −2 V and with a drain bias of −7 V. For clarity, the profiles are shifted over the potential axis. (b) The corresponding transfer curve measured.

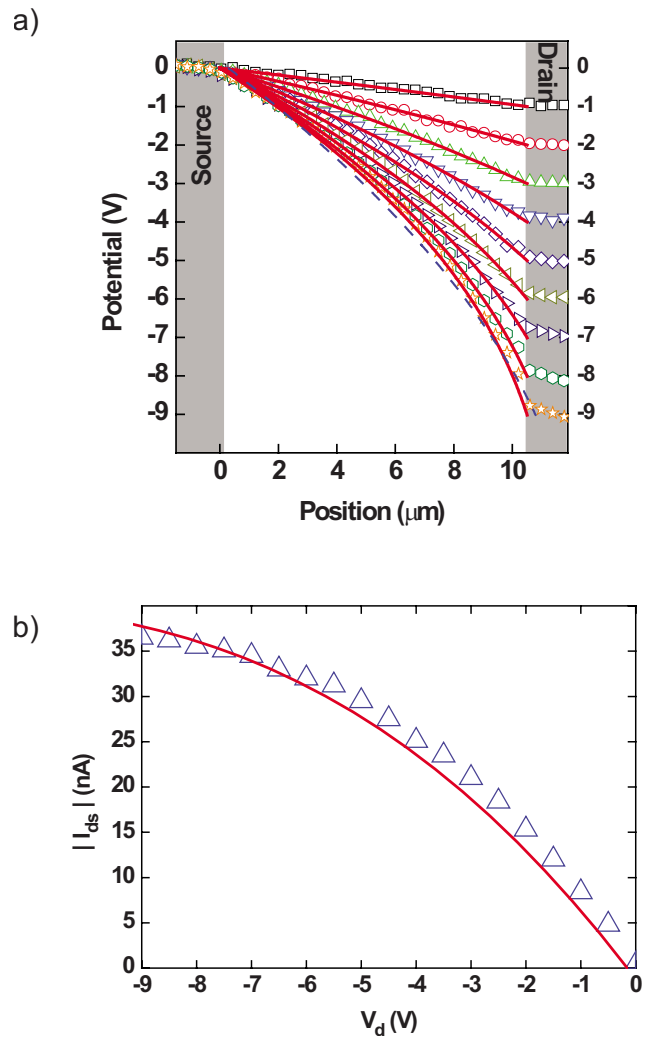

FIG. 3. (Color online) Output curves, together with the corresponding potential profiles, as measured for a unipolar PTAA field-effect transistor. Symbols and solid lines represent measured data points and fits, respectively. (a) The potential profiles measured at a drain bias from −1 to −9 V in steps of −1 V and with a gate bias of −7 V. The dashed line represents the best possible fit at a drain bias of −9 V with a constant mobility (MOS model). (b) The corresponding output curve.

tonically. Therefore, the potential profile is superlinear from source to drain. This development in shape is clearly visible in the output curves of Fig. 3(a).

IV. AMBIPOLAR POTENTIAL PROFILES

A unipolar transistor operates in saturation when $|V_d| > |V_g - V_t|$. The channel is pinched off and charge cannot accumulate in the pinched-off part of the channel. However, in an ambipolar transistor under these bias conditions, the effective gate potential changes sign and gives rise to simultaneous injection of electrons and holes from opposite sides of the channel. A transition region, which acts as a p-n junction, separates the accumulation channels. The width of the junction depends on the recombination rate. For an infinitely large recombination rate, the n- and p-type regions can be seen as an abrupt p-n junction, resulting in a steplike increase in the potential. For a low recombination rate, a first order approximation of the junction is a linearly graded one. The holes and electrons are not as well separated as in the abrupt junction. Therefore, one can show that the steplike increase of the potential broadens.[30] A clear distinction between the low and high recombination rates cannot be made with current-voltage measurements alone.[19] We assume a high recombination rate, leading to a junction that is much narrower than the channel length. The center of the recombination zone is located at $x=x_0$, which is the position where the effective gate potential is zero. The ambipolar transistor is represented by a unipolar n-type transistor with channel length x_0 and a unipolar p-type transistor with channel length L-x_0. Current conservation then implies that the electron current at $x=0$ is equal to the hole current injected at the other

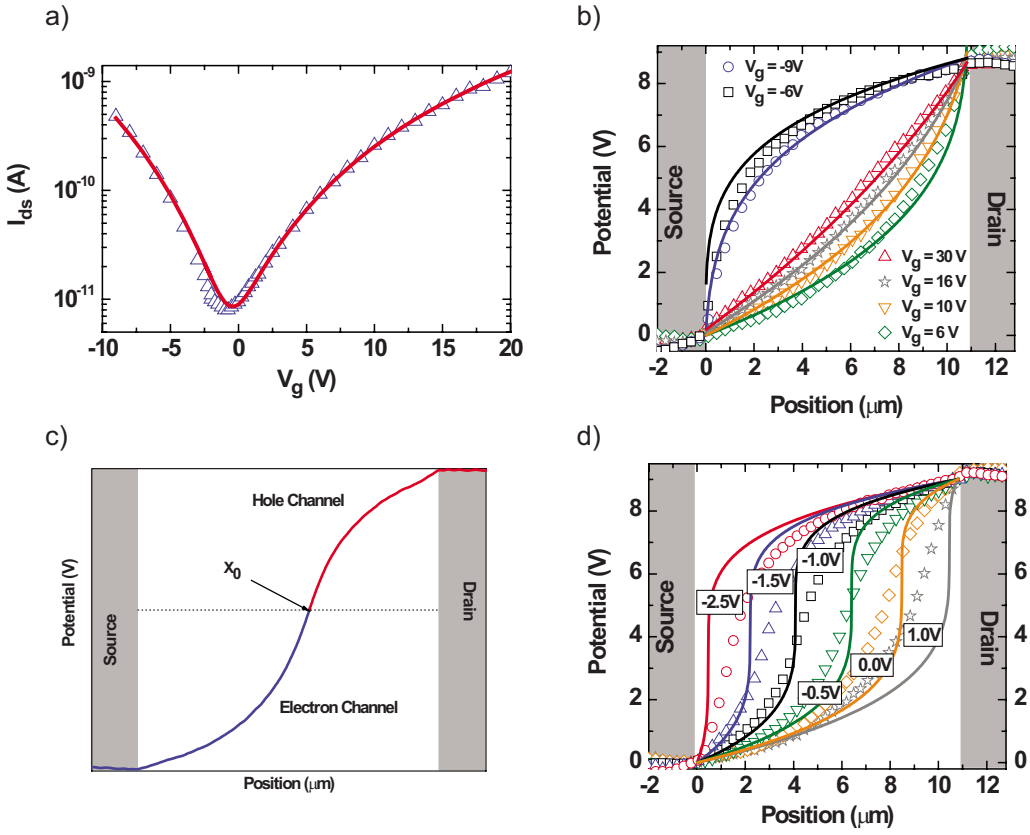

FIG. 4. (Color online) Transfer and output curves, together with the corresponding potential profiles, as measured for an ambipolar NiDT field-effect transistor. Symbols show measured data points. The solid lines are calculated. (a) The transfer curve measured at a drain bias of +9 V. (b) Corresponding potential profiles in electron and hole accumulation modes. (c) Schematic overview of the potential profile as expected for a *p-n* junction. (d) Measured and calculated potential profiles in the ambipolar operating regime.

electrode at $x=L$, and equal to the total device current. This current is given by[19]

$$I_{ds} = \frac{WC_i}{L}\left[\frac{f_{0,e}}{(\beta_e - 1)\beta_e}(V_g - V_t)^{\beta_e} + \frac{f_{0,h}}{(\beta_h - 1)\beta_h}(V_d - V_g + V_t)^{\beta_h}\right]. \tag{3}$$

The position of the recombination plane in the channel is calculated as

$$x_0 = \frac{\frac{f_{0,e}}{(\beta_e - 1)\beta_e}(V_g - V_t)^{\beta_e}}{\frac{f_{0,h}}{(\beta_h - 1)\beta_h}(V_d - V_g + V_t)^{\beta_h} + \frac{f_{0,e}}{(\beta_e - 1)\beta_e}(V_g - V_t)^{\beta_e}} L, \tag{4}$$

where V_t is a single threshold voltage for both channels. The material parameters β and f_0 are defined separately for both holes and electrons. The local potential $V(x)$ can be calculated similarly as for the unipolar case discussed above by noting that the current is constant at each point x in the channel:

$$V(x) = V_g - V_t - \left[(V_g - V_t)^{\beta_e} - \frac{x}{x_0}(V_g - V_t)^{\beta_e}\right]^{1/\beta_e} \quad \text{for } 0 < x < x_0 \tag{5}$$

and

$$V(x) = V_g - V_t + \left[(V_d - V_g + V_t)^{\beta_h} - \frac{L - x}{L - x_0}[(V_d - V_g + V_t)]^{\beta_h}\right]^{1/\beta_h} \quad \text{for } x_0 < x < L. \tag{6}$$

A transfer curve of our ambipolar transistor at a drain bias of +9 V is presented in Fig. 4(a). The transfer curve was fitted to Eq. (3) to determine the parameters needed to calculate the potential profiles and the position of the recombination zone. The threshold voltage V_t can be estimated from the minimum current. When the parameters for holes and electrons are similar, then Eq. (3) shows that a minimum in the current is obtained when $V_g - V_t$ is equal to $V_d/2$. From Fig. 4(a), a threshold voltage of about −6 V is then estimated. When the gate bias is positive and larger than the drain bias, the current is due to electrons. This part of the transfer curve then yields the values for β_e and $f_{0,e}$. Simi-

larly, when the gate bias is more negative than the threshold voltage, the current is carried by holes. That part of the transfer curve yields the values for β_h and $f_{0,h}$. The fully drawn curve in Fig. 4(a) presents the actual fit to the data. The following parameters were found: $V_t=-5.8$ V, $\beta_h=4.1$, $f_{0,h}=1\times10^{-7}$ cm^2/V$^{(2T_0/T-1)}$ s, $\beta_e=3.6$, and $f_{0,e}=2\times10^{-8}$ cm^2/V$^{(2T_0/T-1)}$ s. The values are comparable to those reported previously.[19]

The corresponding measured potential profiles at a drain bias of +9 V are presented as symbols in Fig. 4(b). The potential profiles vary monotonically with position in the channel, indicating that under those bias conditions the current is carried by one type of carrier only. At high positive gate biases, the potential is strongly curved near the drain. This implies that the current is due to electrons that are being injected from the source. Similarly, at high negative gate bias, the potentials are strongly curved at the source. This implies that the current is then due to holes that are being injected from the drain. The potentials were calculated using the same parameter values as derived from the transfer curves. The solid lines in Fig. 4(b) present the calculated potential profiles. Without any additional parameter, a fair agreement is obtained.

When $|V_d|>|V_g-V_t|>0$, electrons and holes are simultaneously injected from opposite sides of the channel. As depicted in Fig. 4(c), one contact injects electrons and the other, holes. At both contacts, the carrier densities are high and, hence, the lateral electric fields are low. In the channel, the electrons and holes recombine. Consequently, the carrier density decreases and the lateral electric field increases. The signature of recombination in the potential profile is, therefore, represented as a small curvature at both contacts and a steep transition in the channel. The maximum in the first derivative gives the position of the recombination plane, x_0.

Experimental potentials are presented in Fig. 4(d). The solid lines are the potentials calculated using the same parameters as found above. Qualitatively, they demonstrate the expected behavior. The discrepancy between predicted and measured potentials is expected to be due to diffusion currents, electrostatics, and a finite recombination rate. The full width at half maximum of the derivative of the experimental potential profiles indicates a width of approximately 3 μm for the *p-n* junction.

From the derivative of the experimental potential profiles in Fig. 4(d), the position of the recombination plane was determined. This position x_0 is presented as a function of gate bias in Fig. 5. At a gate bias of −5 V, x_0 is located at the source contact, which implies that there is no electron channel. Similarly, at a gate bias larger than 3 V, there is no hole channel. In between, the recombination zone can be tuned along the channel. The solid line is calculated using Eq. (4). Good agreement is obtained.

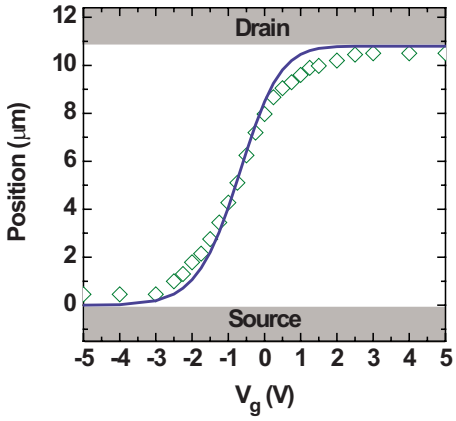

FIG. 5. (Color online) Measured and predicted positions of the *p-n* junction in an ambipolar NiDT field-effect transistor as a function of applied gate bias.

V. CONCLUSION

In conclusion, we have measured charge transport in unipolar and ambipolar OFETs. The potential profiles have been determined by *in situ* SKPM measurements. A model has been derived that predicts simultaneously transport and potentials as functions of gate and drain biases. Transport parameters have been obtained by fitting the transfer curves. Subsequently, without any additional parameters, the potential profiles have been calculated. Good agreement between measured and calculated potentials is obtained. For ambipolar transistors, we find a *p-n* junction, the position of which can be tuned along the channel by the gate bias. The good agreement between measured and calculated data establishes a unified description of charge transport and the complementary potential profiles in field-effect transistors made from disordered organic semiconductors.

ACKNOWLEDGMENTS

The work of E.C.P.S. forms part of the research program of the Dutch Polymer Institute (DPI) Project No. 516. D.M.d.L. and M.C. gratefully acknowledge support of the EU projects NAIMO (NMP4-CT-2004-500355) and PolyApply (IST-IP-507143). The authors are grateful to H. Nulens for his help in setting up the AFM/SKPM, and to R. Coehoorn and D. M. Taylor for fruitful discussions.

*e.c.p.smits@rug.nl

[1] A. Knobloch, A. Manuelli, A. Bernds, and W. Clemens, J. Appl. Phys. **96**, 2286 (2004).

[2] G. H. Gelinck, H. E. A. Huitema, E. van Veenendaal, E. Cantatore, L. Schrijnemakers, J. B. P. H. van der Putten, T. C. T. Geuns, M. Beenhakkers, J. B. Giesbers, B.-H. Huisman, E. J. Meijer, E. Mena Benito, F. J. Touwslager, A. W. Marsman, B. J. E. van Rens, and D. M. de Leeuw, Nat. Mater. **3**, 106 (2004).

[3] P. F. Baude, D. A. Ender, T. W. Kelley, M. A. Haase, D. V. Muyres, and S. D. Theiss, Proceedings of the Device Research

Conference, 2004 (unpublished), Vol. 62, p. 227.
[4] E. Cantatore, T. C. T. Geuns, G. H. Gelinck, E. van Veenendaal, A. F. A. Gruijthuijsen, L. Schrijnemakers, S. Drews, and D. M. de Leeuw, IEEE J. Solid State Circ. **42**, 84 (2007).
[5] V. Subramanian, J. M. J. Frechet, P. C. Chang, A. de la Fuente Vornbrock, D. C. Huang, J. B. Lee, B. A. Mattis, S. Molesa, A. R. Murphy, D. R. Redinger, and S. K. Volkman, Proc. SPIE **5940**, 594013 (2005).
[6] A. R. Brown, C. P. Jarrett, D. M. de Leeuw, and M. Matters, Synth. Met. **88**, 37 (1997).
[7] M. C. J. M. Vissenberg and M. Matters, Phys. Rev. B **57**, 12964 (1998).
[8] M. L. Chabinyc, J.-P. Lu, R. A. Street, Y. Wu, P. Liu, and B. S. Ong, J. Appl. Phys. **96**, 2063 (2004).
[9] A. Salleo and R. A. Street, J. Appl. Phys. **94**, 471 (2003).
[10] R. Schmechel, M. Ahles, and H. von Seggern, J. Appl. Phys. **98**, 084511 (2005).
[11] G. H. Gelinck, E. van Veenendaal, and R. Coehoorn, Appl. Phys. Lett. **87**, 073508 (2005).
[12] E. Calvetti, L. Colalongo, and Zs. M. Kovacs-Vajna, Solid-State Electron. **49**, 567 (2005).
[13] H. Klauk, *Organic Electronics* (Wiley-Interscience, New York, 2006).
[14] G. Horowitz, Adv. Mater. (Weinheim, Ger.) **10**, 365 (1998).
[15] J. S. Swensen, C. Soci, and A. J. Heeger, Appl. Phys. Lett. **87**, 253511 (2005).
[16] J. Zaumseil, R. H. Friend, and H. Sirringhaus, Nat. Mater. **5**, 69 (2006).
[17] E. C. P. Smits, S. Setayesh, T. D. Anthopoulos, M. Buechel, W. Nijssen, R. Coehoorn, P. W. M. Blom, B. de Boer, and D. M. de Leeuw, Adv. Mater. (Weinheim, Ger.) **19**, 734 (2007).
[18] D. L. Smith and P. P. Ruden, Appl. Phys. Lett. **89**, 233519 (2006).
[19] E. C. P. Smits, T. D. Anthopoulos, S. Setayesh, E. van Veenendaal, R. Coehoorn, P. W. M. Blom, B. de Boer, and D. M. de Leeuw, Phys. Rev. B **73**, 205316 (2006).
[20] V. Palermo, M. Palma, and P. Samori, Adv. Mater. (Weinheim, Ger.) **18**, 145 (2005).
[21] L. Bürgi, H. Sirringhaus, and R. H. Friend, Appl. Phys. Lett. **80**, 2913 (2002).
[22] L. Bürgi, R. H. Friend, and H. Sirringhaus, Appl. Phys. Lett. **82**, 1482 (2003).
[23] L. Bürgi, T. J. Richards, M. Chiesa, R. H. Friend, and H. Sirringhaus, Synth. Met. **146**, 297 (2004).
[24] L. Bürgi, T. J. Richards, R. H. Friend, and H. Sirringhaus, J. Appl. Phys. **94**, 6129 (2003).
[25] K. P. Puntambekar, P. V. Pesavento, and C. D. Frisbie, Appl. Phys. Lett. **83**, 5539 (2003).
[26] E. J. Meijer, C. Tanase, P. W. M. Blom, E. van Veenendaal, B.-H. Huisman, D. M. de Leeuw, and T. M. Klapwijk, Appl. Phys. Lett. **80**, 3838 (2002).
[27] J. Veres, S. D. Ogier, S. W. Leeming, D. C. Cupertino, and S. M. Khaffaf, Adv. Funct. Mater. **13**, 199 (2003).
[28] T. D. Anthopoulos, S. Setayesh, E. C. P. Smits, M. Cölle, E. Cantatore, B. de Boer, P. W. M. Blom, and D. M. de Leeuw, Adv. Mater. (Weinheim, Ger.) **18**, 1900 (2006).
[29] C. Tanase, E. J. Meijer, P. W. M. Blom, and D. M. de Leeuw, Org. Electron. **4**, 33 (2003).
[30] S. M. Sze, *Physics of Semiconductor Devices* (Wiley-Interscience, New York, 1981).